Article

Not peer-reviewed version

Insights into the Electrochemical Synthesis and Supercapacitive Behaviour of 3D Copper Oxide-Based Nanostructures

Gintautas Jonkus , Ramunas Levinas * , Natalia Tsyntsaru * , Henrikas Cesiulis

Posted Date: 3 February 2025

doi: 10.20944/preprints202502.0075.v1

Keywords: copper oxides; electrochemical synthesis; 3D nanostructures, electrochemical impedance spectroscopy, specific capacitance

Article

Insights into the Electrochemical Synthesis and Supercapacitive Behaviour of 3D Copper Oxide-Based Nanostructures

Gintautas Jonkus [1], Ramunas Levinas [1,2,*], Natalia Tsyntsaru [1,3,*] and Henrikas Cesiulis [1]

[1] Faculty of Chemistry and Geosciences, Vilnius University, 03225 Vilnius, Lithuania; henrikas.cesiulis@chgf.vu.lt, gintautas.jonkus@gmc.stud.vu.lt

[2] State Research Institute, Center for Physical Sciences and Technology, 10257 Vilnius, Lithuania; ramunas.levinas@ftmc.lt

[3] Institute of Applied Physics, Moldova State University, 2028 Chisinau, Moldova; natalia.tintaru@chgf.vu.lt

* Correspondence: ramunas.levinas@ftmc.lt (R.L.); natalia.tintaru@chgf.vu.lt (N.T.)

Abstract: While renewable energy sources supply a progressively larger share of the world's energetical needs, their non-continuous nature demands coupling with energy storage systems such as batteries or capacitors. Consequently, copper oxide-based materials have emerged as promising candidates due to their affordability, stability, and suitable electrochemical performance. In this study, nanostructured copper oxide-based films were electrochemically synthesized on copper foil and foam electrodes and investigated for their supercapacitive behaviour. The synthesis was carried out via cyclic voltammetry (CV) for up to 1000 cycles in an alkaline electrolyte. By tuning the upper vertex potential (-0.3 V to 0.65 V vs Ag/AgCl), both phase composition (Cu_2O, $Cu(OH)_2$, CuO) and morphology (grains, nanoneedles, nanoplatelets) were precisely controlled, demonstrating the versatility of this approach. EIS data using foil and foam electrodes shows that various processes occur on the electrode during changing potential from -1,0 to 0,6 V and back. The capacitive properties of the synthesized films were evaluated using CV in the potential range of 0 V–0.65 V, and the optimized CuO film synthesized on Cu foam exhibited a high specific capacitance of 2760 mF cm^{-2}. Charge-discharge cycling at 100 mV s^{-1} for 1000 cycles indicated an initial capacitance increase followed by stable retention, highlighting the structural integrity and electrochemical stability of the films. These findings provide valuable insights into the controlled electrochemical synthesis of copper oxide nanostructures and their potential for high-performance capacitor applications.

Keywords: copper oxides; electrochemical synthesis; 3D nanostructures, electrochemical impedance spectroscopy, specific capacitance

1. Introduction

The renewable energy sector is expanding quickly, as demonstrated by the European Union's Green Deal. This initiative aims to make the EU the first climate-neutral region in the world by 2050 [1]. While renewable energy presents numerous advantages, it also faces challenges, mainly due to the non-continuous nature of energy production. This situation stresses the need for more cost-effective energy storage solutions and devices with high capacitance. These materials/devices are becoming increasingly important to meet the rising global demand for efficient energy storage systems that could provide rapid charge and discharge cycles. Many materials have been researched, but most are not readily available or their manufacturing process is complicated [2].

Copper compounds on the other hand can offer sustainable and innovative solutions. Copper is a relatively abundant and cheap metal, and its compounds can be applied to various devices. Thus, copper hydroxide having high specific capacitance was investigated earlier for supercapacitor applications [3]. In addition, cupric oxide (CuO) and cuprous oxide (Cu_2O) have been the subjects of

 doi:10.20944/preprints202502.0075.v1

extensive research, and have emerged as crucial materials in various technological applications due to their remarkable combination of low cost, high chemical stability, and outstanding electrochemical performance [4]. These properties make them particularly appealing in critical areas such as catalysis, photovoltaics, and energy storage. In the context of energy storage, copper oxides are gaining significant attention for their impressive capacitance and responsive electrochemical characteristics, which are essential for developing high-energy supercapacitors [5–7] and the theoretical capacitance of oxides can reach high values: Cu_2O - 2247.6 F/g [8], CuO - 1783 F/g [9].

There is vast published research exploring the latest advancements in the design and application of copper oxide-based nanosystems tailored to enhance electrode materials for next-generation supercapacitors. Thus, different fabrication methodologies were employed to boost the electrode's capacity, including chemical synthesis [10–12], electrostatic coprecipitation [13], hydrothermal synthesis [14], magnetron sputtering [15], ultrasound-assisted fabrication [16] and thermal oxidation among others [17].

Moreover, choosing the fabrication technique for preparing the electrodes is crucial in developing a material with a high surface area [18]. From this perspective, electrochemical synthesis is an efficient technique, that can produce efficient copper oxide-based capacitors [19]. Furthermore, by adjusting the voltage/current, temperature, deposition or cycle duration, solution concentration, and pH level several factors, including the films' crystallographic orientation, thickness, and surface morphology can be controlled [5,6].

Bulk copper oxides exhibit scarce electrical conductivity and have a limited surface area to be employed as commercial energy storage electrodes. Therefore, nanostructured copper oxides have been regarded as offering an easy pathway for electrolyte ion penetration. Different nanostructured morphologies have been proposed, including nanosheets [10,12], nanoparticles [13], nanoflowers [20,21], and nanowires [17,22], which enhance the surface area for ion access from the electrolyte.

Furthermore, commercially available or designed three-dimensional (3D) electrodes, including foams, aerogels, and hydrogels, have been widely studied for electrochemical energy storage applications due to their extensive specific surface areas and outstanding electrochemical properties. They can possess substantial pore volumes to hold a greater quantity of ions, making them very effective as porous electrodes [22].

Despite the wealth of research documented in the literature, there remains a significant gap in our understanding of how to effectively adapt innovative electrochemical designs to yield desirable materials. To address this challenge, our study delves into the controlled synthesis of copper oxide-based films, which are grown on copper foil and foam electrodes. This research aims to explore the most effective scenarios for creating highly nanostructured supercapacitors through a systematic bottom-up approach.

Utilizing the cyclic voltammetry and tuned upper vertex potential, we aim to comprehend the electrochemical dynamics at play. Our findings offer a comprehensive discussion of the electrochemical responses exhibited by various copper oxide-based nanostructures, enriched by valuable insights gleaned from electrochemical impedance spectroscopy measurements. This investigation not only enhances our understanding of these materials but also paves the way for future advancements in energy storage technologies.

2. Materials and Methods

2.1. Synthesis

The copper oxide films were synthesized on copper foil (Roth, 99.5%) and commercial open-cell foam electrodes. The foam had a density of 1.02 g cm^{-3}, a porosity of 87.6% and an approximate ligament diameter of 150–200 μm. Both the foil and foam electrodes were shaped to 1 cm x 1 cm dimensions, having a total geometrical working area from both sides of 2 cm^2. Before synthesis, the electrodes were polished with a commercial detergent, washed well with distilled water, immersed into a 50:50 H_2SO_4: H_2O solution to dissolve surface oxides, and lastly washed well again before

 doi:10.20944/preprints202502.0075.v1

transferring the electrode into the cell. All electrochemical syntheses and measurements were carried out on an Autolab 302N potentiostat (Metrohm, Utrecht, The Netherlands). A three-electrode cell was used, with the copper foil/foam as the working electrode, a saturated Ag/AgCl reference electrode, and a platinized titanium mesh counter electrode. All potentials are reported vs. sat. Ag/AgCl. The syntheses were carried out by cyclic voltammetry (CV) from -1.0 V to different upper vertex potentials (-0.3 V, -0.1V, 0.3 V, 0.6 V and 0.65 V), at a scan rate of 25 mV s^{-1} and in an alkaline 1 M NaOH (Roth, 99.5%) electrolyte.

2.2. Electrochemical Impedance Spectroscopy

Electrochemical Impedance Spectroscopy (EIS) was used to elaborate the copper oxide film growth mechanism on Cu foil electrodes. The spectra were obtained potentiostatically, at 0.1 V increments from -0.6 V to 0.6 V. The frequency range was 15 kHz to 20-50 mHz, and the potential perturbation amplitude was 5 mV. The spectra were interpreted by fitting to equivalent electric circuits.

2.3. Structure and Morphology

The surface morphology of the synthesized copper oxide films was observed using a scanning electron microscope SU-70 (Hitachi, Tokyo, Japan). XRD diffraction patterns were obtained with a Rigaku MiniFlex II X-ray diffractometer (Rigaku, Tokyo, Japan). The average crystallite sizes of identified phases were calculated from the diffractograms by the Halder-Wagner method.

2.4. Evaluation of Capacitive Properties

To evaluate the capacitive properties of the synthesized films, CV scans were carried out in a 1 M NaOH electrolyte at increasing scan rates (5 mV s^{-1}, 10 mV s^{-1}, 25 mV s^{-1}, 50 mV s^{-1} and 100 mV s^{-1}), in the potential range of 0 V to 0.65 V. The charge/discharge stability was evaluated by carrying out 1000 cycles in the same potential range.

3. Results

3.1. Evaluation of Electrochemical Synthesis of Copper Oxide-Based Nanostructures

The synthesis of nanostructured copper-based films on foil and foam electrodes was conducted by cycling the applied potential between -1.0 V (cathodic) and 0.65 V (anodic) for up to 1000 cycles. The resulting curves are presented in Figure 1.

In the case of the foil electrode (Figure 1a), the initial scans reveal three distinct peaks in the anodic part of the CV:

- Peak I, observed at -0.4 V, corresponds to the oxidation of metallic copper (equation 1).
- Peak II, at -0.16 V, is associated with the formation of CuO from Cu_2O (equation 2).
- Peak III, located at -0.01 V, pertains to the direct formation of CuO from metallic copper (equation 3). [23–25].

It must be noted that the formation of hydroxide may occur simultaneously (equation 4), resulting in mixed Cu_2O/CuOH and CuO/$Cu(OH)_2$ phases.

$$2Cu + 2OH^- \rightarrow Cu_2O + H_2O + 2e^- \quad (1)$$

$$Cu_2O + 2OH^- \rightarrow 2CuO + H_2O + 2e^- \quad (2)$$

$$Cu + 2OH^- \rightarrow CuO + H_2O + 2e^- \quad (3)$$

$$CuOH + OH^- \leftrightarrow Cu(OH)_2 + e^- \quad (4)$$

Moreover, the current is rather small during the first 100 cycles at higher anodic potentials, as a relatively passive CuO/$Cu(OH)_2$ layers forms on the surface [26]. However, after 200 cycles a broad

 doi:10.20944/preprints202502.0075.v1

anodic and cathodic current region emerges from 0 V to 0.65 V (Figure 1, peaks IV and cIV). It has been shown that this electrochemical behaviour is caused by the reversible oxidation/reduction of copper oxide and hydroxide species (equations 2 and 4) and such behaviour is reflected in the pseudocapacitive properties of given materials [27,28].

The number of cycles is an important parameter and plays a crucial role in the electrochemical behaviour of the films. It is evident that after 10-20 cycles the peak at -0.01 V can no longer be distinguished, and film formation proceeds mainly through equation 2. In addition, the peak related to this process shifts towards more anodic potentials and peak current density increases. The increased current density is probably associated with the evolving electrochemically active surface area due to nanostructuring (as will be discussed later). In contrast, the peak potential shift signals the changes at the interface electrode/synthesized films.

When carrying out the synthesis on a Cu foam electrode, the process undergoes differently which is reflected in the appearance at the first scan of the pronounced anodic peak at ~ 0.2 V (Figure 1b). This peak is likely caused by the initial formation of copper oxides/hydroxides on the foam electrode's relatively larger electrochemically active surface area. During the subsequent cycling, the peak position returns to more cathodic values in line with the foil electrode (~ 0 V). Interestingly, the peak current values drop as the synthesis proceeds to the final 1000th cycle, which may indicate irreversible oxidation. However, in the 0 V – 0.65 V region, the same broad oxidation/reduction region is observed on the foil electrode, which indicates that the foam electrode would also exhibit capacitive properties.

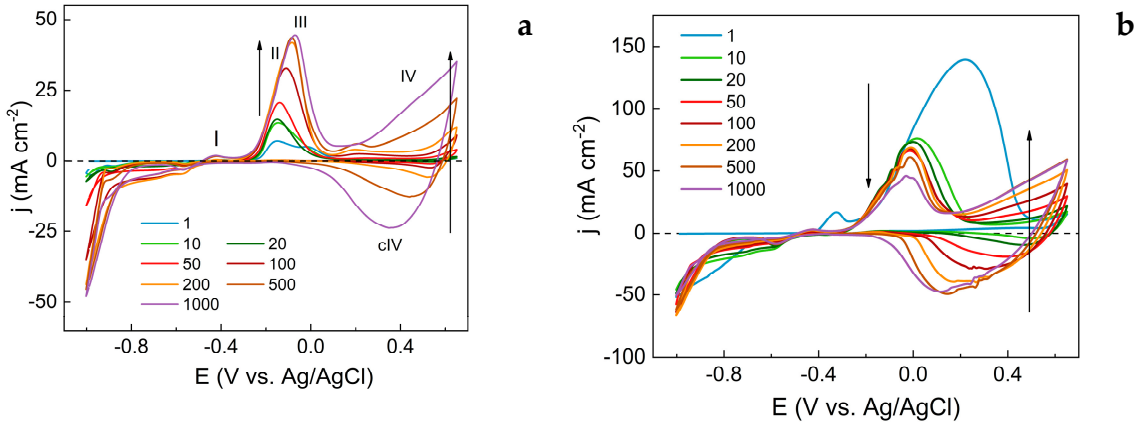

Figure 1. Cyclic voltammetry curves, recorded between -1 V and 0.65 V on Cu foil (a) and foam (b) in 1 M NaOH at various cycles and 25 mV s-1 scan rate. Arrows show trends of current density with cycle number.

To relate synthesis conditions to structural and morphological properties, several syntheses were carried out on foil substrates from -1.0 V to a vertex potential (-0.3 V, -0.1 V, 0.3 V, 0.6 V and 0.65 V) as shown in Figure 2a**.** By conducting synthesis in this manner, the mechanism of oxide formation as outlined in equations 1-4 could be tuned.

For example, when the upper vertex potential was set as -0.3 V, the peak relating to Cu^{2+} formation was not reached. With -0.1 V the current would reverse direction mid-peak, and with 0.3 V the entire peak would be obtained, but the subsequent anodic process would be omitted. Regardless of upper vertex potential, the cycles retained broadly the same profiles, attesting to the excellent reversibility of this system. When the synthesis was carried out on copper foam electrodes (Figure 2b) the same oxidation/reduction peaks could be distinguished, but two major changes were apparent: the current densities were larger, owing to the larger geometrical area of the foam electrode, and the anodic region (at ~ 0 V to 0.65 V) became broader.

 doi:10.20944/preprints202502.0075.v1

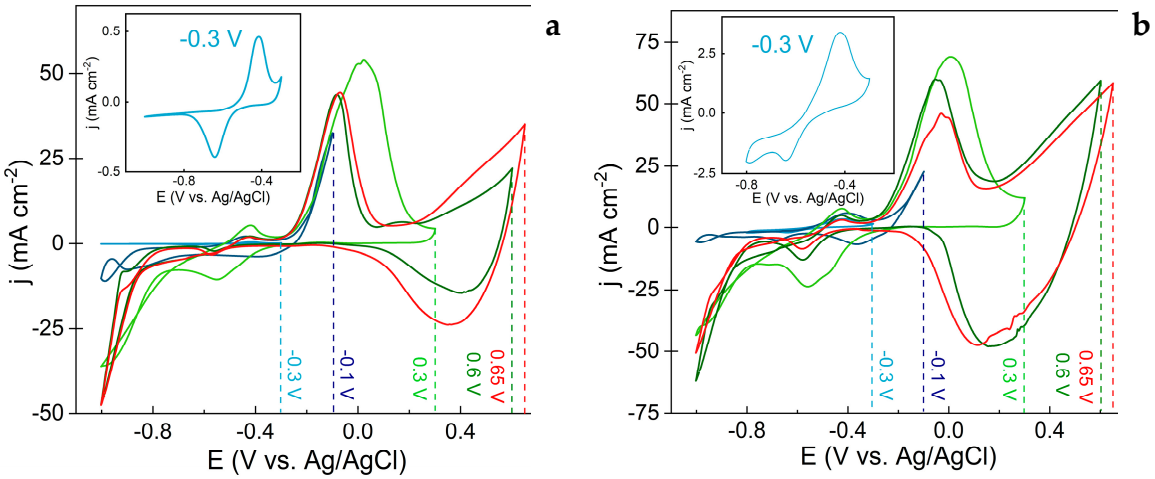

Figure 2. Synthesis of copper-based films after 1000 cycles to various upper vertex potentials (shown with dashed lines) on Cu foil (a) and foam (b) substrates. Inserts are shown magnified image for synthesis at -0.3 V.

A further evaluation of the formation of layers on copper foil and foam electrodes was investigated by electrochemical impedance spectroscopy (EIS) measurements changing the applied potential in steps of 0.1 V from -0.4 to 0.6 V and back. The interpretation of EIS data is based on the process model simulated by the equivalent electric circuits (EEC), where a clear physical meaning is assigned to each passive element. This approach was discussed in detail in [29]. Usually, the design of EEC is based on the presumed processes occurring on the electrode, and the shapes of impedance spectra plotted in Nyquist and Bode coordinates. The number of maxima and plateaus in Bode plots indicates the number of capacitors in EEC, whereas the Nyquist plot is valuable to analyse processes occurred at lower frequencies.

Some examples of conformity of fitted EEC to the obtained EIS in Nyquist and Bode coordinates are presented in Figure 3. Where values of elements at potentials -0.3 V and 0.1 V are:

- R1=1.474 Ω cm²; R2=113.1 Ω cm²; R3=7930 Ω cm²; CPE1=3.737 10^{-5} (F cm^{-2})$^{0.853}$; n1=0.853; CPE2=0.422 (F cm^{-2})$^{0.422}$; n2=0.422 (Figure 3a,b);

R1=1.703 Ω cm²; R2=6431 Ω cm²; CPE1=1.01 10^{-4} (F cm^{-2})$^{0.938}$; n1=0.938; CPE2=0.422 (F cm^{-2})$^{0.804}$; n2=0.804 (Figure 3c,d).

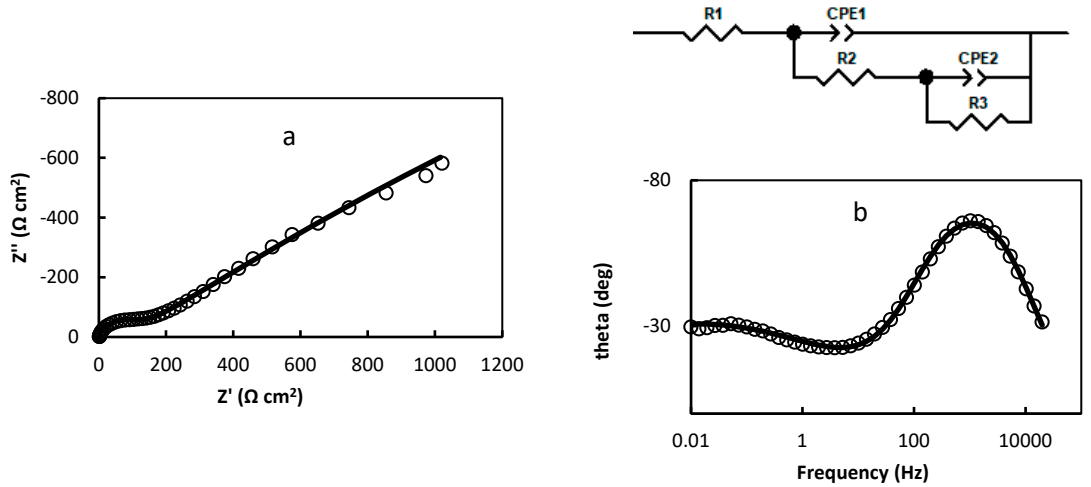

Preprints.org (www.preprints.org) | NOT PEER-REVIEWED | Posted: 3 February 2025 doi:10.20944/preprints202502.0075.v1

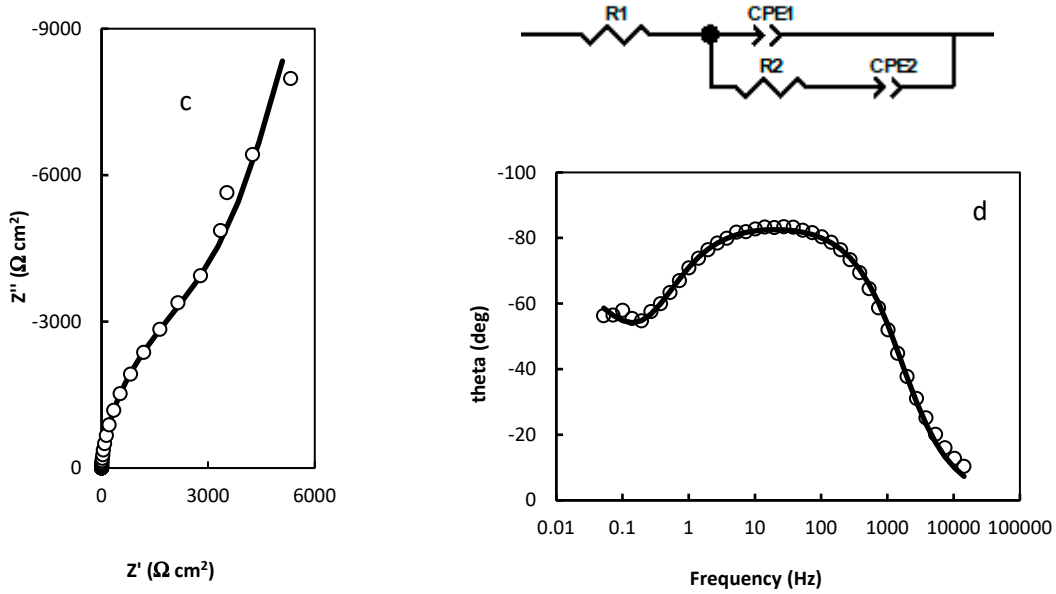

Figure 3. Characteristic EIS presented as Nyquist (a,c) and Bode (b,d) plots obtained on the foil electrode at the potentials -0.3 V (a, b) and 0.1 V (c, d); circles – experimental data, solid lines – results of fitting to the EEC shown above corresponding Bode plots. The EEC used for fitting are in inserts, and values of elements at a given potential are presented in the text.

The different electrochemical processes are obtained in the different potential ranges, and the results of their modelling by EEC and the physical meanings of passive elements in EEC are shown in Figure 4.

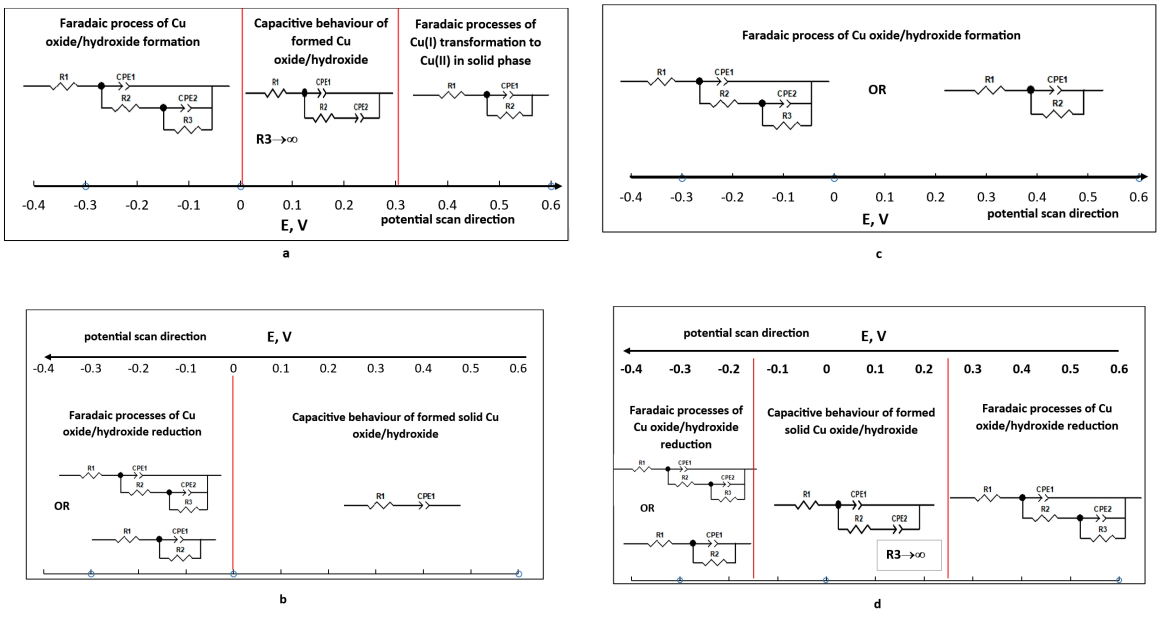

Figure 4. A. Potential ranges of equivalent circuits used to fit experimental EIS spectra obtained on the copper foil (a, b) and foam (c, d) electrodes. The physical meaning of discrete elements: R1 is an uncompensated resistance; CPE1 is a constant phase element modelling a capacitance of a double electric layer; R2 is a charge transfer resistance (or the charge transfer resistance of faster electron transfer reaction); CPE2 and R3 simulate an impedance of sequential charge transfer, where CPE2 and R3 is a constant phase element and charge transfer resistance in the slower reaction, respectively. The red lines indicate the transition to different kinetics.

 doi:10.20944/preprints202502.0075.v1

It is noticeable that the film formation processes occur differently on the foil and foam electrodes (Figure 4). On the foil electrode, anodic film is formed at potentials ranging from -0.4 V to 0.0 V (Figure 4a). Then at the potential ranging from 0.0 V to 0.3 V obtained films exhibit capacitive behaviour, as the values of R3 are approaching infinite, while the charge transfer resistance R2 takes on finite values from 1576 to 78013 Ω cm^2. It means that the direct current can pass through the circuit until the maximum amount of the film is formed.

At more positive anodic potentials another faradaic process is occurring, namely transformations in the solid phase, and the EIS of this process can be modelled by well-known modified Ershler-Randles EEC (Figure 4a). When oxide/hydroxide film on the copper is already formed, and the potential is reducing from 0.6 V to -0.4 V (Figure 4b), the synthesized film shows capacitive behaviour up to a potential of 0.0 V. When the potential further decreases, the reduction of the formed film begins, EIS usually is fitted to the EEC typically described faradaic processes occurring on the electrodes (Figure 4b).

The processes on the foam electrode during anodic-cathodic cycling are the same but the kinetics differ (compare data shown in Figures 1 and 4). When the potential of the foam electrode is changed from -0.4 to 0.6 V (Figure 4c), the faradaic processes occur in the entire range of potentials, because EIS are fitted to the EEC describing a multistage process [29] or to the modified Ershler-Randle EEC.

The formation of anodic films via the faradaic process continues longer on the foam electrode, because of the larger specific surface area, namely, during cycling to the anodic side and then to the cathodic range when the potential is changed from 0.6 V to 0.25 V (Figure 4c,d). In this case, the charge transfer resistance R2 or R2+R3, respectively does not exceed 10000 Ω cm^2. The capacitive behaviour (only R3 approach infinitive) is observed in the potential range narrower than in the foil electrodes, from 0.25 V to -0.15 V (Figure 4d).

3.2. Evaluation of Morphology and Structure of the Obtained Films

SEM observations reveal that surface morphology varies greatly with synthesis conditions and that distinct nanostructures could be obtained by tuning the upper vertex potential. When carrying out synthesis on copper foil substrates, cauliflower-like nanoplatelets were observed for films synthesized at upper vertex potentials of 0.65 V and 0.6 V (Figure 5a,b), whereas continuous arrays of collapsed nanoneedles would form when using more cathodic potentials (0.3 V and -0.1 V, Figure 5c,d).

In literature, comparable nanoneedle formations had been attributed to both copper oxides and hydroxides [30,31]. Similar nanoplatelet and nano-needle surface morphologies also dominate on foam electrodes (Figure 5e-g), but due to the 3D framework and many zones of potentially different local current densities, several distinct types of nanostructures could be observed on these electrodes. Lastly, only a compact surface covering film was obtained when the upper vertex potential was set to -0.1 V (Figure 5h).

 doi:10.20944/preprints202502.0075.v1

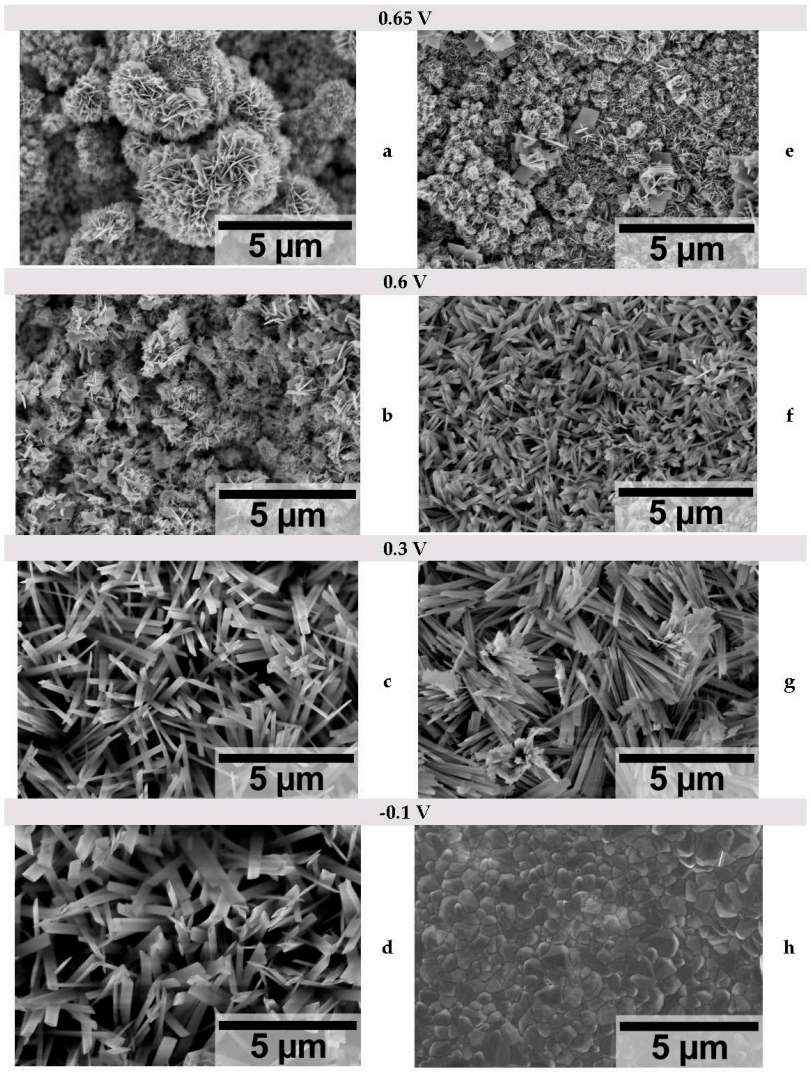

Figure 5. SEM images of copper oxide/hydroxide films after 1000 cycles, synthesized at various upper vortex potentials on Cu film (a, b, c, d) and foam (e, f, g, h) substrates.

Obtained X-ray diffraction patterns reveal that the phase structure of the synthesized films correlates to the upper vertex potential reached during synthesis (Figure 6a). When the films had been synthesized from -1.0 V until the potential of -0.3 V, apart from a strong background signal from the substrate, the diffractogram only contained the (111) and (200) peaks of Cu_2O at 2θ = 36.4 ° and 42.3 ° respectively (ICDD # 00-005-0667). When the upper vertex potential was extended to -0.1 V, additional $Cu(OH)_2$ peaks at 23.7 ° (021), 33.9 ° (002), 35.7 ° (111), 39.8 ° (130) and 52.9 ° (150) emerged (ICDD # 00-003-0310). Also, the intensity of these peaks increased, owing to the larger thickness of the film.

The same Cu_2O and $Cu(OH)_2$ phases could still be observed when the upper vertex potential was 0.3 V, but from here a distinct peak of the (111) face of CuO began to appear at 38.7 °. Subsequently, when the potential was further extended towards 0.6 V and 0.65 V, the (-111) and (111) peaks of CuO at 35.5 ° and 38.7 ° became more intense (ICDD # 00-005-0661), and the peaks related to Cu_2O and $Cu(OH)_2$ disappeared. It is evident that more anodic potentials favour the formation of CuO, and a similar result was reported for Cu anodized potentiostatically in alkaline media [32].

The relation between upper vertex potential and phase structure on films synthesized on foam electrodes is similar to foil electrodes (Figure 6b). Cu_2O dominates when synthesis is carried out until more cathodic potentials, and the CuO phase forms after synthesis to more anodic vertex potentials, with all three (Cu_2O, $Cu(OH)_2$ and CuO) phases existing at intermediate conditions. One noteworthy

 doi:10.20944/preprints202502.0075.v1

difference is that on foam electrodes phase purity is improved, as Cu_2O and $Cu(OH)_2$ are not obtained for the more anodic upper vertex potentials (0.6 V and 0.65 V).

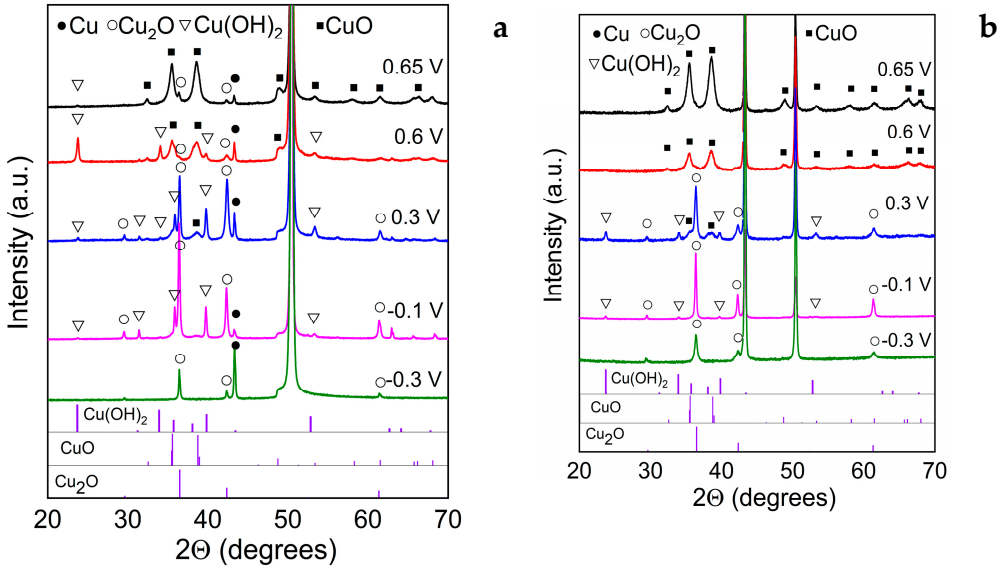

Figure 6. XRD diffractograms of copper oxide and hydroxide films, obtained through cyclic voltammetry after 1000 cycles at various upper vertex potentials on Cu foil (a), and foam (b) substrates.

Table 1 contains the average crystallite sizes of the main identified copper oxide and hydroxide phases, as calculated by the Halder-Wagner method. The respective diffractograms for foil electrodes in Figure 6a show that the CuO peaks are distinctly broader than those of Cu_2O and $Cu(OH)_2$, suggesting the formation of finer crystallites. Where CuO is the dominant phase (when the upper vertex potential was 0.65 V) the average crystallite size was 15 nm. However, when the dominant phases are Cu_2O and $Cu(OH)_2$, their respective crystallite sizes are 46.5 nm to 55.4 nm and 27.0 nm to 33.1 nm. Similar crystallite sizes have been reported in the literature for copper oxides and hydroxides, albeit synthesized by other methods [33,34].

As mentioned before, phase purity was improved when synthesizing CuO on foam electrodes, and for the highest upper vertex potential syntheses (0.6 V and 0.65 V) only the CuO phase could be detected. However, here the CuO crystallites were even finer – 9.1 nm. The crystallite sizes of Cu_2O and $Cu(OH)_2$ were also appreciably smaller where these phases could be reliably identified. It therefore seems that more nanocrystalline films are obtained on copper foam electrodes, which can impact the capacitive properties of these films.

Table 1. Average crystallite sizes of XRD identified copper compounds, synthesized by the cyclic voltammetry on copper foil and foam electrodes at different upper vortex potentials (E_{max}).

	Crystallite size, nm					
	Foil			Foam		
E_{max}, V	Cu_2O	$Cu(OH)_2$	CuO	Cu_2O	$Cu(OH)_2$	CuO
0.65	-	-	10.9	-	-	9.1
0.6	-	27.6	13.3	-	-	9.1
0.3	35.1	35.0	10.2	23.2	23.4	9.6
-0.1	37.0	35.0	-	39.8	37.8	-
-0.3	17.7	-	-	6.4	-	-

 doi:10.20944/preprints202502.0075.v1

3.3. Evaluation of Capacitive Properties

The capacitive properties of the most promising films were further evaluated by carrying out cyclic voltammetry at increasing scan rates in the pseudocapacitive region of 0 V to 0.65 V as shown in Figure 7. As briefly discussed before, the charge accumulation and release properties of these copper oxide materials are caused not the by charge/discharge of the electrical double layer, but instead by reversible oxidation/reduction reactions (equations 5 – 8) [35].

$$CuO + H_2O + 2e^- \leftrightarrow Cu_2O + 2OH^- \quad (5)$$

$$Cu_2O + H_2O + 2OH^- \leftrightarrow 2Cu(OH)_2 + 2e^- \quad (6)$$

$$CuOH + OH^- \leftrightarrow 2Cu(OH)_2 + e^- \quad (7)$$

$$CuOH + OH^- \leftrightarrow CuO + H_2O + e^- \quad (8)$$

For this reason, the cyclic voltammograms are not of a perfect square shape that would be characteristic for double layer capacitors, and instead these electrodes should be thought of as reversible pseudocapacitors [17,36,37]. Interestingly, the film that had been synthesized to the upper vertex potential of 0.65 V does not display the expected increase of current density with faster potential scan rates over the entire potential range (Figure 7a). Instead, the cyclic voltammograms become "narrower" at faster scan rates, which signals either slow oxidation/reduction kinetics (e.g., as per equations 5-8), or impeded charge transfer from the substrate towards the interface. This issue is mitigated when characterizing the pseudocapacitive properties of the films, synthesized to 0.3 V and -0.3 V (Figure 7b,c**)**. Here higher potential scan rates result in larger current densities over the entire measured potential range, which is characteristic of faster charge transfer. The same general trends hold for the films, synthesized on foam substrates (Figure 7d-f).

Here the current densities are larger, owing to the larger surface area of the 3D framework of the foam electrode. It also becomes apparent that in some cases the oxidation/reduction reactions are not perfectly reversible, as is the case for the film that had been synthesized on Cu foam to an upper vertex potential of -0.3 V (Figure 7f). The anodic part of the cycle is far larger than the cathodic part (e.g., at 50 mV s^{-1} Q_{anodic} = 0.13 C; $Q_{cathodic}$ = 0.03), which means that during synthesis the film's structure or morphology had not yet reached equilibrium, and oxidation reactions still dominate. For comparison, for foam electrodes synthesized to 0.65 V and 0.3 V, the anodic and cathodic charges for the 50 mV s^{-1} cycle are respectively: Q_{anodic} = 0.35 C, $Q_{cathodic}$ = 0.34 C, and Q_{anodic} = 0.19 C, $Q_{cathodic}$ = 0.18 C).

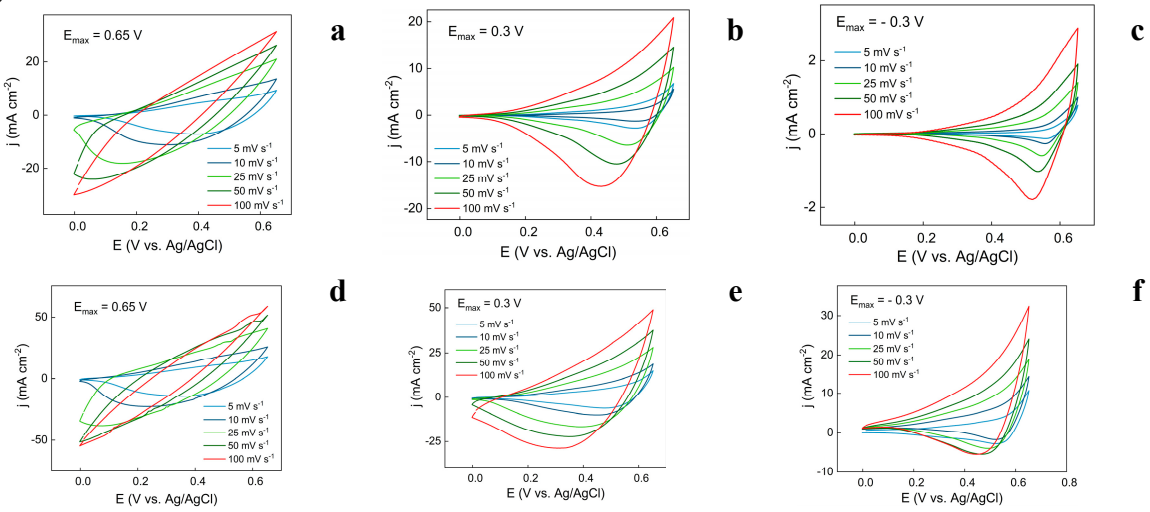

 doi:10.20944/preprints202502.0075.v1

Figure 7. Cyclic voltammetry curves showcasing the pseudocapacitive behaviour of nanostructured copper oxide-based films, synthesized on copper foil (a, b, c) and foam (d, e, f) electrodes at different upper vertex potentials (E_{max}) and scan rates.

To better compare the different systems, the specific aerial capacitances were calculated by equation 9 [38]:

$$C_s = \frac{1}{2Av(V_c - V_a)} \int_{V_a}^{V_c} I(V)dV \quad (9)$$

Here C_s is the specific capacitance per surface area (F cm^{-2}), v is the potential scan rate (V s^{-1}), V_c and V_a are the cathodic and anodic vertex potentials respectively (0 V and 0.65 V), and the integral represents the total area of the j-E curve. Note, that because of the complex nature of the synthesis, the active mass could not be reliably estimated. Therefore, the mass component of the specific capacitance equation was exchanged for surface area (A, cm^2), which is sometimes called the aerial specific capacitance.

Figure 8 depicts the calculated specific capacitances of the synthesized films as measured under different potential scan rates. Firstly, it is evident that slower scan rates result in significantly larger specific capacitances – a consequence of the relatively slow charge/discharge process, most likely related to the intricate nanostructuring of the surface. The largest specific capacitance obtained in this study is 2760 mF cm^{-2} (0.65 V foam electrode, at 5 mV s^{-1}). This is comparable and even improves over some values that had been reported for copper oxide nanostructures in literature: 1641.4 mF cm^{-2} [35], 1954 mF cm^{-2} [39], 3348.5 mF cm^{-2} [40]. The specific capacitances calculated for foam electrodes are larger than for foil electrodes due to the open-cell nature and 3D nanostructuring of the substrate.

Additionally, the specific capacitances of films synthesized to more cathodic vertex potentials were also characterized (Figure 8b,c). It is observed that the total C_s values are much smaller on both foil and foam electrodes. However, the decrease of C_s with increasing potential scan rate can also be inferred to be smaller. Then, the following conclusion can be made: due to intricate nanostructuring and favourable phase structure, the films synthesized to more anodic upper vertex potentials (0.65 V) exhibit higher total specific capacitances but impeded charge transfer kinetics limit their charge/discharge rate. Meanwhile, the films synthesized to more cathodic upper vertex potentials (0.3 V, -0.3 V) have lower specific capacitances, but faster charge/discharge kinetics.

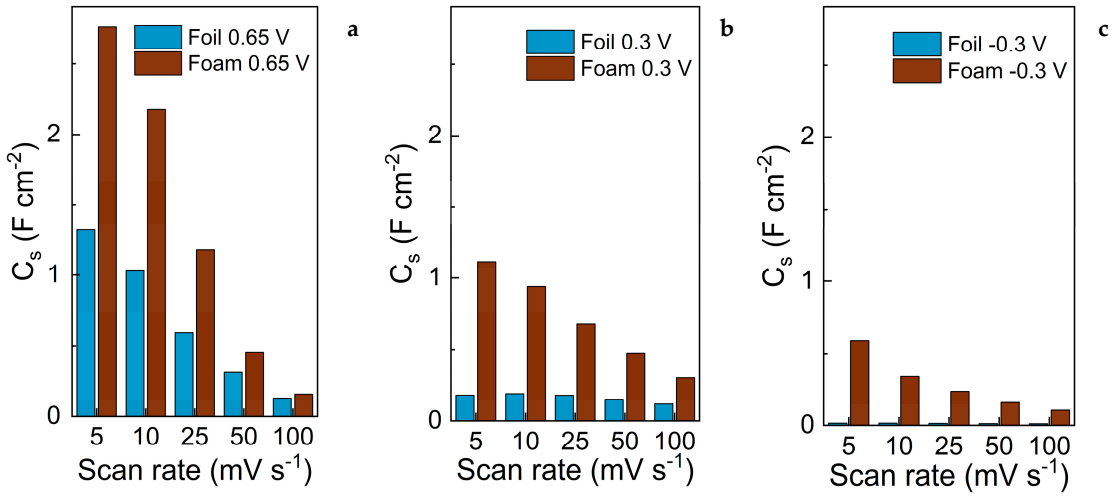

Figure 8. Calculated specific capacitances of films, synthesized on copper foil and foam electrodes, to different upper vertex potentials: 0.65 V (a), 0.3 V (b) and -0.3 V (c).

Lastly, we examined the stability of the best-performing electrode by carrying out 1000 CV scans at the fastest potential scan rate of 100 mV s^{-1} and observed that it exhibits excellent cycle reproducibility for the duration of this test (Figure 9a). It was also noted that, although visually the

 doi:10.20944/preprints202502.0075.v1

cycles appear identical, the specific capacitance trends toward higher values over the first 500 cycles, and subsequently plateaus (Figure 9b). These observations indicate that the restructuring of the surface structure or morphology continues, but a stable equilibrium is eventually reached, allowing the system to function as an efficient pseudocapacitor.

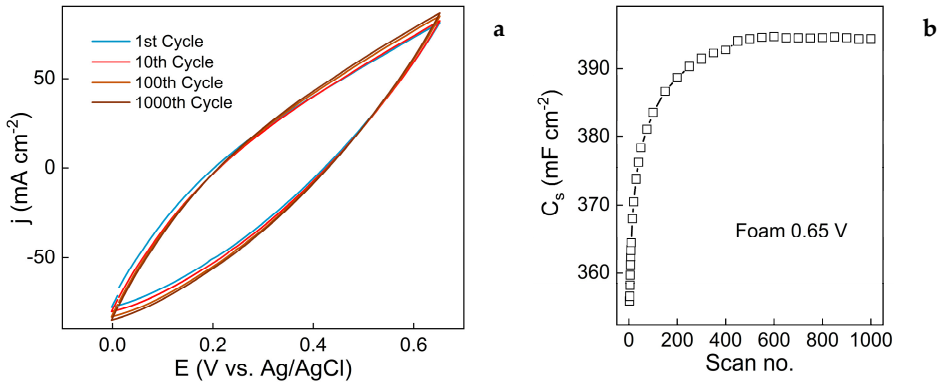

Figure 9. Characterization of capacitive stability of Cu foam electrode, synthesized to upper vertex potential of 0.65 V: CV scans obtained at 100 mV s^{-1} (a), change of C_s with the number of scans.

4. Conclusions

In this study, nanostructured copper oxide films were electrochemically synthesized on copper foil and foam substrates, and their application as oxidation/reduction pseudocapacitors was characterized. The synthesis was carried out by performing cyclic voltammetry scans from a lower vertex potential of -1.0 V to a variable upper vertex potential (from -0.3 V to 0.65 V). It was observed that limiting the upper vertex potential during synthesis would result in films with different phase structures – more cathodic potentials limited the oxidation products to just Cu_2O, whereas more anodic potentials yielded $Cu(OH)_2$ and CuO. EIS data using foil and foam electrodes shows that various processes occur on the electrode during changing potential from -1,0 to 0,6 V and back: faradaic processes of Cu oxide/hydroxide formation, capacitive behaviour of formed films, faradaic processes of transformation in solid state. The obtained EIS data was successfully interpreted in terms of EEC applied for data fitting.

The surface morphology could also be tuned from featureless-grained, to nanoneedles and nanoplatelets, showcasing the utility of this synthesis method to obtain nanostructured copper oxide films. The capacitive properties of the synthesized films were characterized by cyclic voltammetry in the 0 V – 0.65 V range at different scan rates, and specific capacitances were calculated. Due to the 3D framework of the substrate, on foam electrodes, the specific capacitances were larger when accounting for the geometrical surface area of the electrode. A specific capacitance value of 2760 mF cm^{-2} was obtained for the film, synthesized on Cu foam to an upper vertex potential of 0.65 V when measured at a 5 mV s^{-1} scan rate. The charge/discharge stability of this film was evaluated for 1000 cycles at 100 mV s^{-1} scan rate, and it was observed that the specific capacitance grows until an equilibrium value, after which the capacitive properties are completely retained until the end of the experiment.

Author Contributions: Conceptualization and methodology, R.L., H.C. and N.T.; investigation, G.J., R.L.; writing—original draft preparation, R.L., H.C. and N.T.; writing—review and editing, all; visualization, R.L., H.C. and N.T. All authors have read and agreed to the published version of the manuscript.

Funding: This study was partially funded by the Vilnius University, and the Moldavian National project ANCD project 011204.

Data Availability Statement: data supporting reported results will be available upon request from the authors.

Conflicts of Interest: The authors declare no conflicts of interest.

 doi:10.20944/preprints202502.0075.v1

References

1. Delivering the European Green Deal. Https://Commission.Europa.Eu/Strategy-and-Policy/Priorities-2019-2024/European-Green-Deal/Delivering-European-Green-Deal_en 2025.
2. Sisakyan, N.; Chilingaryan, G.; Manukyan, A.; Mukasyan, A.S. Combustion Synthesis of Materials for Application in Supercapacitors: A Review. *Nanomaterials* **2023**, *13*, 3030, doi:10.3390/nano13233030.
3. Gurav, K.V.; Patil, U.M.; Shin, S.W.; Agawane, G.L.; Suryawanshi, M.P.; Pawar, S.M.; Patil, P.S.; Lokhande, C.D.; Kim, J.H. Room Temperature Chemical Synthesis of Cu(OH)2 Thin Films for Supercapacitor Application. *Journal of Alloys and Compounds* **2013**, *573*, 27–31, doi:10.1016/j.jallcom.2013.03.193.
4. Majumdar, D.; Ghosh, S. Recent Advancements of Copper Oxide Based Nanomaterials for Supercapacitor Applications. *Journal of Energy Storage* **2021**, *34*, 101995, doi:10.1016/j.est.2020.101995.
5. Patake, V.D.; Joshi, S.S.; Lokhande, C.D.; Joo, O.-S. Electrodeposited Porous and Amorphous Copper Oxide Film for Application in Supercapacitor. *Materials Chemistry and Physics* **2009**, *114*, 6–9, doi:10.1016/j.matchemphys.2008.09.031.
6. Sadale, S.B.; Patil, S.B.; Teli, A.M.; Masegi, H.; Noda, K. Effect of Deposition Potential and Annealing on Performance of Electrodeposited Copper Oxide Thin Films for Supercapacitor Application. *Solid State Sciences* **2022**, *123*, 106780, doi:10.1016/j.solidstatesciences.2021.106780.
7. Patil, S.S.; Pawar, S.M.; Ghatage, S.V.; Patil, A.P.; Redekar, R.S.; Yadav, H.M.; Tarwal, N.L.; Patil, P.S. Charge Storage Dynamics and Time Series Analysis of Binder Free Rapidly Synthesized Copper Oxide for Supercapacitors. *Materials Science in Semiconductor Processing* **2024**, *184*, 108769, doi:10.1016/j.mssp.2024.108769.
8. Xu, P.; Liu, J.; Liu, T.; Ye, K.; Cheng, K.; Yin, J.; Cao, D.; Wang, G.; Li, Q. Preparation of Binder-Free CuO/Cu2O/Cu Composites: A Novel Electrode Material for Supercapacitor Applications. *RSC Adv.* **2016**, *6*, 28270–28278, doi:10.1039/C6RA00004E.
9. Singh, B.K.; Shaikh, A.; Dusane, R.O.; Parida, S. Copper Oxide Nanosheets and Nanowires Grown by One-Step Linear Sweep Voltammetry for Supercapacitor Application. *Journal of Energy Storage* **2020**, *31*, 101631, doi:10.1016/j.est.2020.101631.
10. Dubal, D.P.; Dhawale, D.S.; Salunkhe, R.R.; Jamdade, V.S.; Lokhande, C.D. Fabrication of Copper Oxide Multilayer Nanosheets for Supercapacitor Application. *Journal of Alloys and Compounds* **2010**, *492*, 26–30, doi:10.1016/j.jallcom.2009.11.149.
11. Viswanathan, A.; Shetty, A.N. Facile In-Situ Single Step Chemical Synthesis of Reduced Graphene Oxide-Copper Oxide-Polyaniline Nanocomposite and Its Electrochemical Performance for Supercapacitor Application. *Electrochimica Acta* **2017**, *257*, 483–493, doi:10.1016/j.electacta.2017.10.099.
12. Shinde, S.; Dhaygude, H.; Kim, D.-Y.; Ghodake, G.; Bhagwat, P.; Dandge, P.; Fulari, V. Improved Synthesis of Copper Oxide Nanosheets and Its Application in Development of Supercapacitor and Antimicrobial Agents. *Journal of Industrial and Engineering Chemistry* **2016**, *36*, 116–120, doi:10.1016/j.jiec.2016.01.038.
13. Pendashteh, A.; Mousavi, M.F.; Rahmanifar, M.S. Fabrication of Anchored Copper Oxide Nanoparticles on Graphene Oxide Nanosheets via an Electrostatic Coprecipitation and Its Application as Supercapacitor. *Electrochimica Acta* **2013**, *88*, 347–357, doi:10.1016/j.electacta.2012.10.088.
14. Wang, Q.; Zhang, Y.; Xiao, J.; Jiang, H.; Hu, T.; Meng, C. Copper Oxide/Cuprous Oxide/Hierarchical Porous Biomass-Derived Carbon Hybrid Composites for High-Performance Supercapacitor Electrode. *Journal of Alloys and Compounds* **2019**, *782*, 1103–1113, doi:10.1016/j.jallcom.2018.12.235.
15. Pawar, S.M.; Kim, J.; Inamdar, A.I.; Woo, H.; Jo, Y.; Pawar, B.S.; Cho, S.; Kim, H.; Im, H. Multi-Functional Reactively-Sputtered Copper Oxide Electrodes for Supercapacitor and Electro-Catalyst in Direct Methanol Fuel Cell Applications. *Sci Rep* **2016**, *6*, 21310, doi:10.1038/srep21310.
16. Majumdar, D.; Baugh, N.; Bhattacharya, S.K. Ultrasound Assisted Formation of Reduced Graphene Oxide-Copper (II) Oxide Nanocomposite for Energy Storage Applications. *Colloids and Surfaces A: Physicochemical and Engineering Aspects* **2017**, *512*, 158–170, doi:10.1016/j.colsurfa.2016.10.010.
17. Morariu (Popescu), M.-I.; Nicolaescu, M.; Hulka, I.; Duțeanu, N.; Orha, C.; Lăzău, C.; Bandas, C. Fabrication of Cu2O/CuO Nanowires by One-Step Thermal Oxidation of Flexible Copper Mesh for Supercapacitor Applications. *Batteries* **2024**, *10*, 246, doi:10.3390/batteries10070246.

18. Dubal, D.P.; Gund, G.S.; Lokhande, C.D.; Holze, R. CuO Cauliflowers for Supercapacitor Application: Novel Potentiodynamic Deposition. *Materials Research Bulletin* **2013**, *48*, 923–928, doi:10.1016/j.materresbull.2012.11.081.
19. Sayyed, S.G.; Shaikh, A.V.; Shinde, U.P.; Hiremath, P.; Naik, N. Copper Oxide-Based High-Performance Symmetric Flexible Supercapacitor: Potentiodynamic Deposition. *J Mater Sci: Mater Electron* **2023**, *34*, 1361, doi:10.1007/s10854-023-10738-7.
20. Xu, W.; Dai, S.; Liu, G.; Xi, Y.; Hu, C.; Wang, X. CuO Nanoflowers Growing on Carbon Fiber Fabric for Flexible High-Performance Supercapacitors. *Electrochimica Acta* **2016**, *203*, 1–8, doi:10.1016/j.electacta.2016.03.170.
21. Xi, Y.; Xiao, Z.; Lv, H.; Sun, H.; Zhai, S.; An, Q. Construction of CuO/Cu-Nanoflowers Loaded on Chitosan-Derived Porous Carbon for High Energy Density Supercapacitors. *Journal of Colloid and Interface Science* **2023**, *630*, 525–534, doi:10.1016/j.jcis.2022.10.037.
22. Luan, V.H.; Han, J.H.; Kang, H.W.; Lee, W. Highly Porous and Capacitive Copper Oxide Nanowire/Graphene Hybrid Carbon Nanostructure for High-Performance Supercapacitor Electrodes. *Composites Part B: Engineering* **2019**, *178*, 107464, doi:10.1016/j.compositesb.2019.107464.
23. Shu, X.; Zheng, H.; Xu, G.; Zhao, J.; Cui, L.; Cui, J.; Qin, Y.; Wang, Y.; Zhang, Y.; Wu, Y. The Anodization Synthesis of Copper Oxide Nanosheet Arrays and Their Photoelectrochemical Properties. *Applied Surface Science* **2017**, *412*, 505–516, doi:10.1016/j.apsusc.2017.03.267.
24. Wan, Y.; Wang, X.; Sun, H.; Li, Y.; Zhang, K.; Wu, Y. Corrosion Behavior of Copper at Elevated Temperature. *International Journal of Electrochemical Science* **2012**, *7*, 7902–7914, doi:10.1016/S1452-3981(23)17963-6.
25. Teo, W.Z.; Ambrosi, A.; Pumera, M. Direct Electrochemistry of Copper Oxide Nanoparticles in Alkaline Media. *Electrochemistry Communications* **2013**, *28*, 51–53, doi:10.1016/j.elecom.2012.12.006.
26. Caballero-Briones, F.; Artés, J.M.; Díez-Pérez, I.; Gorostiza, P.; Sanz, F. Direct Observation of the Valence Band Edge by in Situ ECSTM-ECTS in p-Type Cu_2O Layers Prepared by Copper Anodization. *J. Phys. Chem. C* **2009**, *113*, 1028–1036, doi:10.1021/jp805915a.
27. Vidhyadharan, B.; Misnon, I.I.; Aziz, R.A.; Padmasree, K.P.; Yusoff, M.M.; Jose, R. Superior Supercapacitive Performance in Electrospun Copper Oxide Nanowire Electrodes. *J. Mater. Chem. A* **2014**, *2*, 6578–6588, doi:10.1039/C3TA15304E.
28. Pawar, S.M.; Kim, J.; Inamdar, A.I.; Woo, H.; Jo, Y.; Pawar, B.S.; Cho, S.; Kim, H.; Im, H. Multi-Functional Reactively-Sputtered Copper Oxide Electrodes for Supercapacitor and Electro-Catalyst in Direct Methanol Fuel Cell Applications. *Sci Rep* **2016**, *6*, 21310, doi:10.1038/srep21310.
29. Cesiulis, H.; Tsyntsaru, N.; Ramanavicius, A.; Ragoisha, G. The Study of Thin Films by Electrochemical Impedance Spectroscopy. In *Nanostructures and Thin Films for Multifunctional Applications*; Tiginyanu, I., Topala, P., Ursaki, V., Eds.; NanoScience and Technology; Springer International Publishing: Cham, 2016; pp. 3–42 ISBN 978-3-319-30197-6.
30. Oyarzún, D.P.; Tello, A.; Sánchez, J.; Boulett, A.; Linarez Pérez, O.E.; Martin-Trasanco, R.; Pizarro, G.D.C.; Flores, M.; Zúñiga, C. Exploration of Copper Oxide Nanoneedle Electrosynthesis Applied in the Degradation of Methylene Blue. *Nanomaterials* **2021**, *11*, 2994, doi:10.3390/nano11112994.
31. Li, F.; Wang, M.; Kong, M.; Tao, S.; Zhang, C.; Wang, K. Synthesis and Growth Features of Copper Hydroxide Iodide Nanoneedles. *Materials Letters* **2007**, *61*, 846–849, doi:10.1016/j.matlet.2006.06.001.
32. Kumar, S.K.; Murugesan, S.; Suresh, S. Anodization Assisted Preparation of Diverse Nanostructured Copper Oxide Films for Solar Selective Absorber. *Optical Materials* **2023**, *135*, 113304, doi:10.1016/j.optmat.2022.113304.
33. Rajani, C.; Anuradha, V.; Sunandamma, Y. Copper Oxide/Hydroxide Nanomaterial Synthesized from Simple Copper Salt. *Int. J. Nanosci.* **2020**, *19*, 1950028, doi:10.1142/S0219581X19500285.
34. Dörner, L.; Cancellieri, C.; Rheingans, B.; Walter, M.; Kägi, R.; Schmutz, P.; Kovalenko, M.V.; Jeurgens, L.P.H. Cost-Effective Sol-Gel Synthesis of Porous CuO Nanoparticle Aggregates with Tunable Specific Surface Area. *Sci Rep* **2019**, *9*, 11758, doi:10.1038/s41598-019-48020-8.
35. He, D.; Xing, S.; Sun, B.; Cai, H.; Suo, H.; Zhao, C. Design and Construction of Three-Dimensional Flower-like CuO Hierarchical Nanostructures on Copper Foam for High Performance Supercapacitor. *Electrochimica Acta* **2016**, *210*, 639–645, doi:10.1016/j.electacta.2016.05.196.

36. Liu, J.; Wang, J.; Xu, C.; Jiang, H.; Li, C.; Zhang, L.; Lin, J.; Shen, Z.X. Advanced Energy Storage Devices: Basic Principles, Analytical Methods, and Rational Materials Design. *Advanced Science* **2018**, *5*, 1700322, doi:10.1002/advs.201700322.
37. Conway, B.E. Transition from "Supercapacitor" to "Battery" Behavior in Electrochemical Energy Storage. *J. Electrochem. Soc.* **1991**, *138*, 1539–1548, doi:10.1149/1.2085829.
38. Sayyed, S.G.; Shaikh, A.V.; Shinde, U.P.; Hiremath, P.; Naik, N. Copper Oxide-Based High-Performance Symmetric Flexible Supercapacitor: Potentiodynamic Deposition. *J Mater Sci: Mater Electron* **2023**, *34*, 1361, doi:10.1007/s10854-023-10738-7.
39. He, D.; Wang, G.; Liu, G.; Suo, H.; Zhao, C. Construction of Leaf-like CuO–Cu_2 O Nanocomposites on Copper Foam for High-Performance Supercapacitors. *Dalton Trans.* **2017**, *46*, 3318–3324, doi:10.1039/C7DT00287D.
40. Wang, S.; Hu, J.; Jiang, L.; Li, X.; Cao, J.; Wang, Q.; Wang, A.; Li, X.; Qu, L.; Lu, Y. High–Performance 3D CuO/Cu Flowers Supercapacitor Electrodes by Femtosecond Laser Enhanced Electrochemical Anodization. *Electrochimica Acta* **2019**, *293*, 273–282, doi:10.1016/j.electacta.2018.09.144.